Comprehensive Analysis of Hexagonal Sigma-Delta Modulations for Three-Phase High-Frequency VSC Based on Wide-Bandgap Semiconductors

David Lumbreras, *Graduate Student Member, IEEE*, Jordi Zaragoza, *Member, IEEE*, Néstor Berbel, Juan Mon, Eduardo Gálvez, and Alfonso Collado

***Abstract*—The efficiency of wide-bandgap (WBG) power converters can be greatly improved using high-frequency modulation techniques. This article proposes using single-loop and double-loop hexagonal sigma-delta (H-ΣΔ and DH-ΣΔ, respectively) modulations for voltage source converters (VSC) that use silicon carbide (SiC) semiconductors. These allow high switching frequencies to operate more efficiently than silicon devices. Thus, ΣΔ modulations are excellent candidates for taking advantage of WBG devices. The proposed modulation techniques allow working with a variable switching frequency, thus producing an extreme reduction in switching losses and mitigating the low-order harmonics in comparison with the classical space vector pulsewidth modulation (SVPWM) technique, and with the innovative variable switching frequency pulse-width modulation (VSFPWM). The performance and losses of both ΣΔ techniques are analyzed here using MATLAB/Simulink and PLECS, and then compared with SVPWM and VSFPWM. Furthermore, the frequency spectrum and the total harmonic distortion are evaluated. Experimental results performed on a VSC converter that uses SiC MOSFETs show how H-ΣΔ and DH-ΣΔ greatly improve efficiency and generate fewer low-order harmonics than the SVPWM and VSFPWM strategies do.**

***Index Terms*—Hexagonal quantizer, losses, modulation techniques, PLECS, power electronics, sigma-delta (ΣΔ) modulation, vector quantization, voltage source converter (VSC), wide-bandgap (WBG) semiconductors.**

Manuscript received July 3, 2020; revised September 21, 2020; accepted November 11, 2020. Date of publication November 23, 2020; date of current version February 5, 2021. This work was supported in part by the Industrial Doctorates Plan of the Secretaria d'Universitats i Recerca del Departament d'Empresa i Coneixement de la Generalitat de Catalunya and in part by the Ministerio de Ciencia, Innovación y Universidades of Spain, under Project PID2019-111420RB-I00. Recommended for publication by Associate Editor J. He. *(Corresponding author: David Lumbreras.)*

David Lumbreras is with the Terrassa Industrial Electronics Group, Department of Electronic Engineering, Technical University of Catalonia (UPC), 08222 Terrassa, Spain, and also with the R&D Power Electronics, Circutor S.A., 08232 Viladecavalls, Spain (e-mail: david.lumbreras@upc.edu).

Jordi Zaragoza, Néstor Berbel, and Juan Mon are with the Terrassa Industrial Electronics Group, Department of Electronic Engineering, Technical University of Catalonia (UPC), 08222 Terrassa, Spain (e-mail: jordi.zaragoza-bertomeu@upc.edu; nestor.berbel-artal@upc.edu; juan.mon@upc.edu).

Eduardo Gálvez and Alfonso Collado are with the R&D Power Electronics, Circutor S.A., 08232 Viladecavalls, Spain (e-mail: egalvez@circutor.com; acollado@circutor.com).

Color versions of one or more of the figures in this article are available at https://doi.org/10.1109/TPEL.2020.3039630.

Digital Object Identifier 10.1109/TPEL.2020.3039630

I. Introduction

WIDE-BANDGAP (WBG) semiconductors display material properties that are superior to those of silicon devices. These new materials surpass silicon in every aspect: they can withstand higher voltages and temperatures while working at extremely high switching frequencies [1], [2]. The most mature WBG semiconductors are silicon carbide (SiC) and gallium nitride (GaN), but recent advances have been made through research into other materials [3]. In general, GaN technology exhibits better features than SiC, but this is currently in its first development stages [4]. Thus, GaN devices are limited to low-voltage applications (<650 V), whereas SiC devices are preferred for high-voltage operations [2]. WBG devices have already been successfully used on several power electronics applications, such as wireless chargers [5], [6], onboard EV chargers [7], [8], energy storage systems [9], shipboard electrification [10], and ac electric drives [11]. Furthermore, two-level SiC converters, such as voltage source converters (VSCs) (see Fig. 1), are becoming the preferred topology in electric vehicles [12]. SiC-based VSCs have also been proposed for uninterruptible power supplies [13], and even to connect an aircraft's generator to its electrical grid [14]. Nevertheless, the industry is not fully taking advantage of WBG properties. In order to exploit the capability of switching at high frequencies with minor losses, WBG power converters should use modulation techniques that provide better results at those frequencies, such as through spread spectrum modulations [15].

There are four types of spread-spectrum-based pulsewidth modulation techniques: random modulations, periodic modulations, programmed modulations, and chaotic modulations [15]. Some works proposed a variable switching frequency pulsewidth modulation (VSFPWM) as an alternative to the classic spread-spectrum techniques [16], [17]. This technique has been adapted to work with ac drives [18], [19], three-level converters, and T-type converters [20]. The VSFPWM technique has proved its effectiveness at low switching frequencies. Compared with a space vector pulsewidth modulation (SVPWM), the VSFPWM reduces the conducted electromagnetic interferences (EMIs) and the switching losses [16], [17]. However, this technique has not been tested at high frequencies, so its applicability for WBG power converters has not been studied.

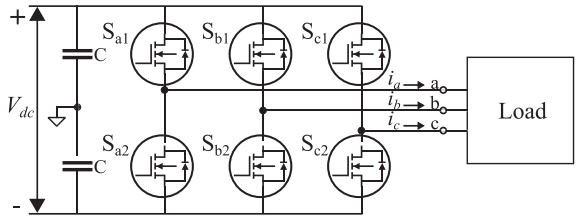

Fig. 1. VSC with SiC MOSFETs.

Another interesting modulation technique is sigma-delta (ΣΔ) modulation, which first appeared in the early 1960s [21], [22]. Nowadays, it is used in audio applications, digital-to-analog converters, sample-rate converters, and digital power amplifiers [23]. The basis of ΣΔ is the following [21]: an analog signal is sampled and compared with the current digital output. The integral of the error is quantized into a digital signal, which is the next output of the modulator. An error usually occurs between the output signal and the quantifier input, but the resolution is easily improved by oversampling the signal, specifically by sampling the analog input at a frequency higher than the Nyquist frequency [21]–[23]. Other popular methods for improving the resolution of ΣΔ are increasing the integrators, which may destabilize the system [24], and using cascade modulators, which are more complex to implement and limited to low-voltage applications [21], [25].

Power converters are like analog-to-digital converters because they receive analog signals as reference voltages and modulate them by means of discrete switching states [26]. In power electronics, it is usual to sample the signals at the switching frequency, which is much higher than the Nyquist frequency. Hence, applying ΣΔ in power converters guarantees a high oversampling ratio and, therefore, good resolution [26].

ΣΔ modulation first appeared in power electronics in [27] as an application for resonant power converters. The performance of this technique was studied in [28] for single-phase and three-phase resonant converters. Later, some authors applied ΣΔ to VSCs and also studied its frequency spectrum [29], [30]. Luckjiff *et al.* improved the modulation by using a hexagonal quantizer [26], when they invented and patented hexagonal ΣΔ (H-ΣΔ) modulation [31]. The same authors analyzed the spectrum and switching rate of their new modulation in [32] and [33]. Furthermore, these authors studied the effects of the double-loop hexagonal ΣΔ (DH-ΣΔ) modulation for power electronics applications in [26] and [34]. Other works extended the study of H-ΣΔ by comparing this technique with space vector modulation (SVM) [35]. Finally, a variation of (H-ΣΔ) known as space vector ΣΔ (SVΣΔ) modulation was presented recently in [36]. This last technique has been applied in three-level converters [37] and multilevel converters [38], [39]. Nevertheless, all these previous works apply ΣΔ and their variants using insulated-gate bipolar transistors (IGBT) at low sampling frequencies of 20 kHz, at maximum. Only in [40], the authors study the effect of another ΣΔ variant at high switching frequencies, the dynamic hysteresis ΣΔ modulation (DHSDM). The DHSDM is simulated in a VSC based on GaN transistors switching at 2 MHz.

Applying ΣΔ at such low sampling frequencies has some important drawbacks. As we mentioned before, a high oversampling ratio improves the resolution of the modulations. Thus, at low sampling frequencies, the error of synthesized voltages may be significant. Moreover, the variable switching frequency of ΣΔ modulations spreads the switching harmonics over a broad frequency range. A low sampling frequency generates low-order harmonics in the output voltages, but the harmonics are displaced to higher frequencies as the oversampling ratio increases [22], [23]. To filter out these low-order harmonics, power converters should have bulky output inductances, which limits the applicability of ΣΔ converters for energy injection into the grid.

Although ΣΔ modulations are usually used in audio applications, their use is scarce in power electronics. Thus, there are no complete studies about the efficiency of these techniques, their losses, nor about the produced total harmonic distortion (THD). Since the few previous studies are performed at low frequencies, the studies about the voltage frequency spectrum are also limited.

This article studies and proposes the use of H-ΣΔ and DH-ΣΔ with a high oversampling ratio for a VSC based on WBG semiconductors (see Fig. 1). The proposed modulations allow the following:

1) working with a variable switching frequency and, consequently, reducing the switching losses;
2) mitigating the low-order harmonics.

Moreover, we perform a theoretical study of H-ΣΔ and DH-ΣΔ with stability, efficiency, and spectral analyses. The stability analysis studies how to tune the parameters of H-ΣΔ and DH-ΣΔ techniques to keep the system stable and minimize the output noise. The efficiency analysis includes a study of the commutations and converter losses. The spectral analysis studies the frequency spectrum and THD. The impact of both ΣΔ strategies is evaluated on the basis of simulation studies using the software MATLAB/Simulink and PLECS. Finally, the results are experimentally validated by implementing the proposed techniques on a VSC converter. To show the benefits of the proposed ΣΔ techniques over other modulation techniques, at high frequency operation, this article compares these techniques with the conventional SVPWM and also with the VSFPWM.

The rest of this article is organized as follows. Section II introduces H-ΣΔ and DH-ΣΔ modulations and analyzes their basis. Section III compares the behavior of the proposed techniques with that of SVPWM and VSFPWM. Section IV validates the above results that showed the impact of the modulation techniques on real power converters. Finally, Section V summarizes the conclusion of this article.

II. Basis of the Method

The scheme of the proposed ΣΔ techniques is shown in Fig. 2. H-ΣΔ is drawn using solid black lines, whereas the dashed red lines mark the extra elements present in DH-ΣΔ. Both techniques have the same structure, but DH-ΣΔ has an additional feedback loop and an integrator.

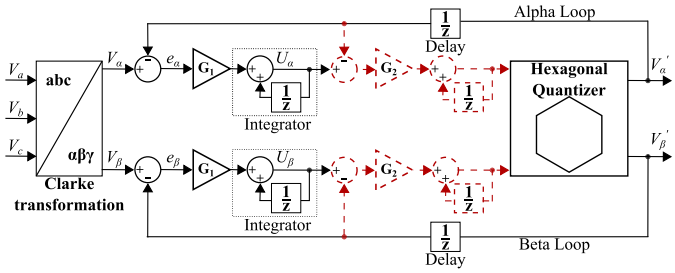

Fig. 2. Hexagonal ΣΔ modulator loop. The second integrator loop is drawn with dashed red lines. The nominal value of all gains is unity.

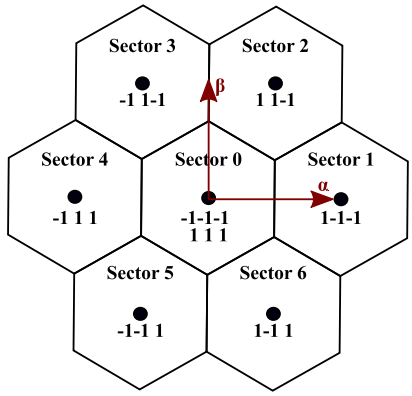

Fig. 3. Two-level vector diagram divided into sectors according to a hexagonal quantizer.

The proposed modulation techniques work in $\alpha\beta$ coordinates; the inputs of both modulations are the reference voltages in *abc* frame, so it is necessary to express them in $\alpha\beta$ coordinates using Clarke's transformation given as

$$\begin{bmatrix} V_\alpha(t) \\ V_\beta(t) \\ V_\gamma(t) \end{bmatrix} = \frac{2}{3} \begin{bmatrix} 1 & -\frac{1}{2} & -\frac{1}{2} \\ 0 & \frac{\sqrt{3}}{2} & -\frac{\sqrt{3}}{2} \\ \frac{1}{2} & \frac{1}{2} & \frac{1}{2} \end{bmatrix} \begin{bmatrix} V_a(t) \\ V_b(t) \\ V_c(t) \end{bmatrix}. \tag{1}$$

These techniques compare the references (V_α, V_β) to the outputs of the quantizer (V'_α, V'_β) and integrate the resulting errors (e_α, e_β). There are gains before each integration, whose value may be adjusted for guaranteeing low output noise and system stability [24]. This is further studied in Section II-A. The integrated errors are the inputs of the hexagonal quantizer, whose outputs are compared to the next reference vector. The equation that describes a single-loop ΣΔ is

$$V'_x(z) = V_x(z)z^{-1} + e_x(z)(1 - z^{-1}) \tag{2}$$

where $x = \{\alpha, \beta\}$. Notice that the quantifier type does not affect the formula.

Increasing the number of integrators is a common practice for improving ΣΔ modulations. DH-ΣΔ has two integrators, and the input of the second loop is the integrated error. Thus, a double-loop ΣΔ is defined using

$$V'_x(z) = V_x(z)z^{-1} + e_x(z)(1 - 2z^{-1} + z^{-2}). \tag{3}$$

The number of integrators can be extended to any number, but in practice, the modulation may become noisy when using three or more integrators [24]. For any number of integrators, (2) is rewritten as

$$V'_x(z) = V_x(z)z^{-1} + e_x(z)(1 - z^{-1})^N \tag{4}$$

where N is the number of integrators.

The hexagonal quantizer is the core of the proposed modulation techniques. The quantizer divides the $\alpha\beta$ plane into seven hexagonal sectors, which are the Voronoi cells of a VSC's eight switching vectors [33]. The switching states are represented by -1 and 1, which indicate, respectively, the output voltage levels of $\frac{-V_{dc}}{2}$ and $\frac{V_{dc}}{2}$ that correspond to the midpoint of the dc bus. Fig. 3 depicts the division of the $\alpha\beta$ plane according to H-ΣΔ.

The quantizer input (i.e., the integrated error) is a random vector in $\alpha\beta$ coordinates that follows the reference vector [36]. At every sampling instant, the hexagonal quantizer determines the position of the input and synthesizes it by applying the nearest switching vector. Since the $\alpha\beta$ plane is a Euclidean space, the switching vector that is closest to the input is found with

$$D_i^2 = (V'_{\alpha i} - U_\alpha)^2 + (V'_{\beta i} - U_\beta)^2 \tag{5}$$

where D_i^2 is the Euclidean distance squared from the integrated error (U_α, U_β) to the switching state $(V_{\alpha i}, V'_{\beta i})$. Calculating D_i^2 instead of simply D_i allows an easier implementation of the quantizer since it avoids the complex square root operation.

The point that is closest to the reference is the switching vector with the minimum value of D_i^2. There are two methods for obtaining the nearest point. The first method is to calculate the distance from the reference to all switching vectors, and the nearest vector is the point with the minimum distance. The second method uses a branch and bound algorithm [41], which allows reducing the number of calculations for finding the closest point. Fig. 4 illustrates the implemented branch and bound algorithm.

Finally, the switching state of the inverter is determined from the output of the quantizer. This procedure is direct, except when the integrated error is within Sector 0. In this case, the converter has to apply one of the two zero vectors (-1-1-1 or 111). Both vectors produce the same output voltages, but the selection affects the converter losses. The proposed techniques aim to minimize losses; thus, they select the vector that reduces the number of switchings in each case. The flowchart of the proposed H-ΣΔ and DH-ΣΔ is depicted in Fig. 4.

A. Stability Analysis

To study the system stability, this article uses the model depicted in Fig. 5. The quantizer is represented as a source of noise. For stability purposes, it is assumed that the noise $E(z)$ is zero.

The closed-loop transfer functions are obtained from this model. The closed-loop transfer function of an H-ΣΔ modulation is

$$G_{\text{cl(H-ΣΔ)}} = \frac{G_1 z}{z - 1 + G_1} \tag{6}$$

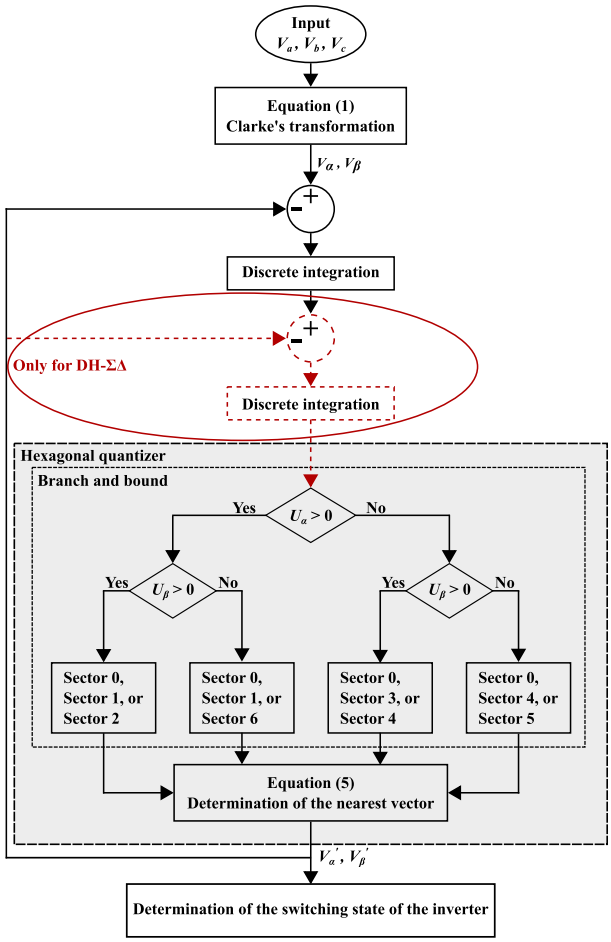

Fig. 4. Flowchart of the proposed ΣΔ techniques. The second integrator loop is drawn with dashed red lines.

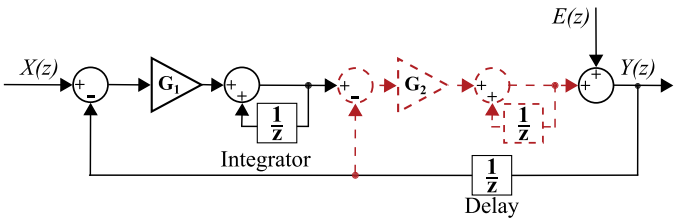

Fig. 5. Generic model of a digital ΣΔ modulation. The second integrator loop is drawn with dashed red lines.

while the transfer function of a DH-ΣΔ modulation is

$$G_{\text{cl(DH-}\Sigma\Delta)} = \frac{G_1 G_2 z^2}{z^2 + ((1+G_1)G_2 - 2)z - G_2 + 1}. \quad (7)$$

The system stability is determined using the previous equations. The gains G_1 and G_2 affect the system stability and may increase output noise. These gains are nominally unity, but circuit imperfections can change these values. If the gains are equal to 1, they do not generate additional noise. The noise increases as the values of gains increase or decrease [24]. Therefore, the gains must be as close to one as possible. However, if the gains are exactly 1, there are pole–zero cancelations, which may cause problems.

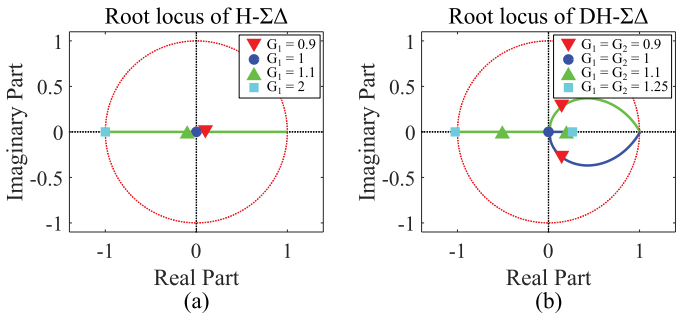

Fig. 6. Root locus analysis, using different gains of (a) H-ΣΔ and (b) DH-ΣΔ.

Fig. 6 illustrates the z-plane of the proposed modulations using different gains. Fig. 6(a) depicts the pole map of H-ΣΔ. The value of G_1 affects to the poles and, thus, to the stability. The system becomes unstable at $G_1 = 2$. Fig. 6(b) shows the poles of DH-ΣΔ. In this map, the two gains are equal and vary from 0.9 to 1.25. The DH-ΣΔ always has two zeros in 0, whereas the poles vary depending on G_1 and G_2. The system becomes unstable at $G_1 = G_2 = 1.236$. DH-ΣΔ allows less gain variation than H-ΣΔ does.

III. Simulation Results

This section evaluates the impact of the proposed H-ΣΔ and DH-ΣΔ techniques on the VSC with SiC MOSFETs in Fig. 1. To assess the effects of the proposed modulations, the results are compared with those of the SVPWM and the VSFPWM strategies.

An important difference between SVPWM, VSFPWM, and ΣΔ techniques is the switching frequency. Since this parameter is variable in VSFPWM, H-ΣΔ, and DH-ΣΔ, this work uses the maximum switching frequency as a comparison parameter. The maximum switching frequency ($f_{\max}$) is defined as follows:

$$f_{\max} = \begin{cases} f_{\text{sw}} & \text{for SVPWM} \\ f_s & \text{for VSFPWM} \\ f_s/2 & \text{for H-}\Sigma\Delta \text{ and DH-}\Sigma\Delta \end{cases} \quad (8)$$

where f_{sw} is the switching frequency and f_s is the sampling frequency.

The VSFPWM requires fixing other parameters: the minimum frequency and the required current ripple. In this work, the minimum frequency is set to half the maximum. The required current ripple is fixed to be the same than those of SVPWM in the same conditions.

The studied VSC is modeled using MATLAB/Simulink and PLECS Blockset. The rated power of the converter is 24.4 kVA, the dc bus voltage is 830 V, and the ac-side currents are constant at their rated values (30 A). The SiC MOSFET module CCS050M12CM2 is used to simulate the converter switches. This module features a maximum drain–source voltage (V_{ds}) of 1.2 kV and a continuous drain current (I_d) of 87 A. Each SiC MOSFET has an external gate resistance of 10 Ω, and their junction

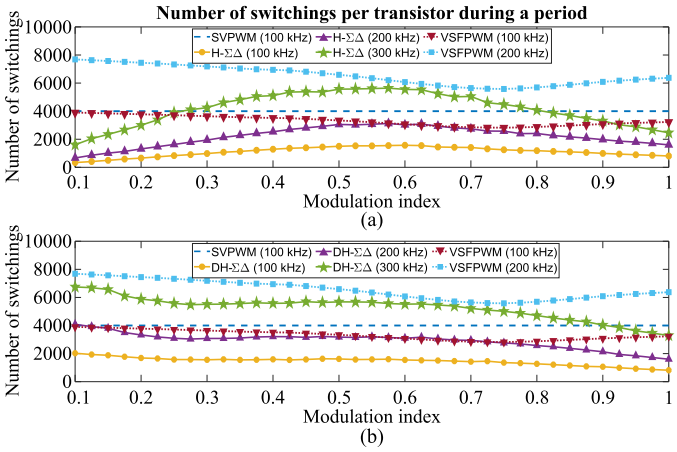

Fig. 7. Comparison of transistor switchings during a period using (a) H-ΣΔ and PWM techniques and (b) DH-ΣΔ and PWM modulations.

temperatures are 125 °C. The PLECS software calculates the losses according to the thermal datasheet and the equations provided by the manufacturer [42].

A. *Efficiency Analysis*

This section analyzes the efficiency of the proposed techniques under various operating conditions. To do this, we first analyzed the commutations. In a fixed-frequency modulation technique, such as SVPWM, the number of commutations per transistor ($\mathrm{No_{sw}} = 2f_{\mathrm{sw}}/f_o$) depends on the switching frequency and the fundamental frequency (f_o). However, the switching frequency is variable in VSFPWM, H-ΣΔ, and DH-ΣΔ as is the number of commutations.

Fig. 7 illustrates the number of switchings produced by the H-ΣΔ and DH-ΣΔ techniques. Fig. 7(a) compares the number of H-ΣΔ switchings to those of SVPWM and VSFPWM. The modulation index (m) affects the number of commutations when we apply H-ΣΔ, and the maximum number of switchings is always between 0.5 and 0.6. The number of commutations is also affected by the maximum frequency; thus, these two parameters are proportional. In general, the H-ΣΔ technique exhibits fewer commutations than SVPWM and VSFPWM. For some operating conditions at 200 kHz, H-ΣΔ switches slightly more than VSFPWM does at 100 kHz, which means they produce equal losses. At 300 kHz, H-ΣΔ exhibits lower commutations than VSFPWM at 200 kHz for all operating points. Furthermore, at high modulation indexes from 0.8 onward, this technique shows fewer switchings than the SVPWM at 100 kHz. Fig. 7(b) compares the commutations of DH-ΣΔ at different frequencies with SVPWM and VSFPWM at 100 kHz. In this case, the number of switchings decreases as the modulation index increases. This technique exhibits more commutations than H-ΣΔ at low modulation indexes. However, from $m = 0.4$ upward, only minor differences exist between the numbers of switchings for both ΣΔ techniques at all the studied frequencies.

Fig. 8 plots the ratio of the total losses of the converter, specifically by comparing the H-ΣΔ and DH-ΣΔ strategies

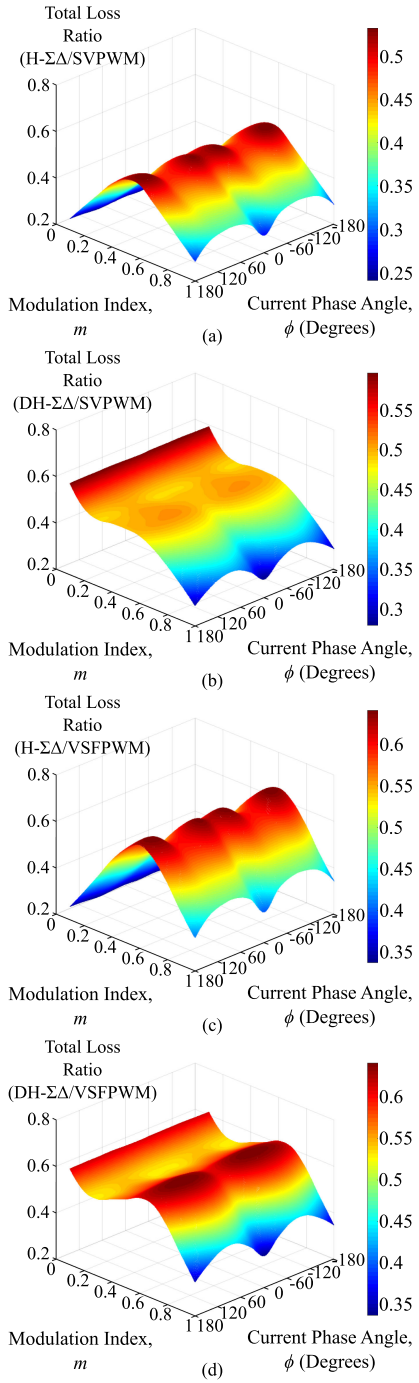

Fig. 8. Ratio of total losses at $f_{\mathrm{max}} = 200$ kHz. (a) and (b) Ratios with SVPWM. (c) and (d) Ratios with VSFPWM.

to SVPWM and VSFPWM. Fig. 8(a) and (b) illustrates the comparison with the SVPWM technique. As shown in Fig. 8(a), the total losses of H-ΣΔ are smaller than those produced by SVPWM under all operating conditions. Fig. 8(b) shows equivalent results for the DH-ΣΔ technique. In this scenario, the reduction in losses is similar to in the previous one. However, DH-ΣΔ causes more switchings than H-ΣΔ at low modulation indexes. Hence, H-ΣΔ exhibits better performance at those operating points. Fig. 8(c) and (d) displays the comparison with

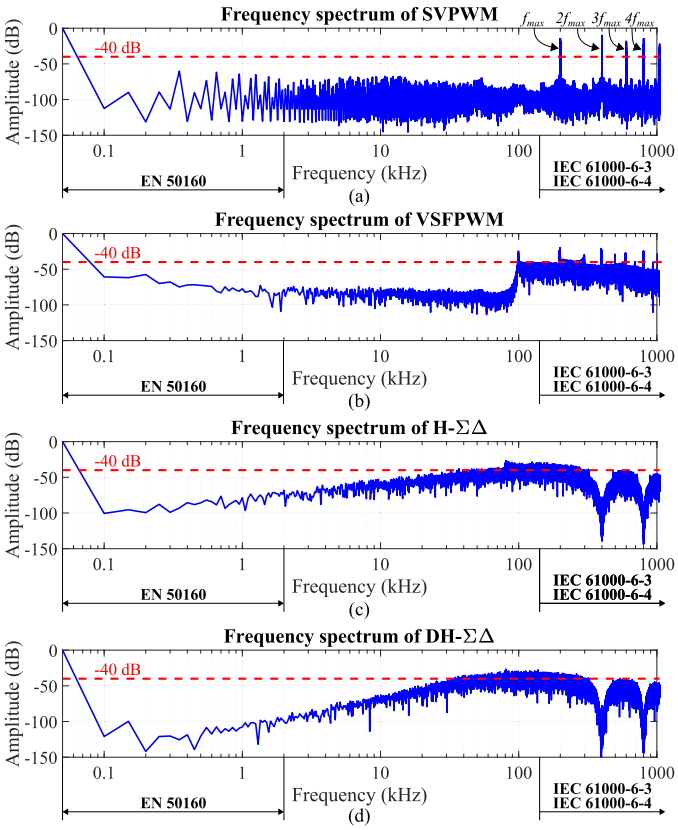

Fig. 9. Frequency spectrum of line voltage (V_{ab}) using (a) SVPWM, (b) VSFPWM, (c) H-ΣΔ, and (d) DH-ΣΔ. Modulation index: $m = 0.8$. Maximum frequency: $f_{\max} = 200$ kHz. The dashed red line marks −40 dB.

the VSFPWM modulation. For all operating conditions, both modulations show fewer losses than VSFPWM. Again, H-ΣΔ exhibits better performance than DH-ΣΔ at low modulation indexes, since the first produces fewer commutations. However, since the VSFPWM produces fewer losses than the SVPWM technique, these ratios are overall higher.

B. Spectral Analysis

This section studies the frequency spectrum of the proposed techniques, including the harmonic distribution and the voltage THD. The results are given in relative units of either dB or %, with the values having been measured from the fundamental voltage.

Fig. 9 illustrates the frequency spectrum of all the studied modulations. These spectra contain three different parts. The first part covers the first 40 harmonics ranging from 0 to 2 kHz. The standard EN 50160 limits the emissions inside this range [43], which are usually harmonics. The second part ranges from 2 to 150 kHz. No standards exist for limiting the EMIs at these frequencies, but this article considers an attenuation of −40 dB to be acceptable. The last range begins at 150 kHz and is covered by two international standards: IEC 61000-6-3 and IEC 61000-6-4 [44], [45]. EMIs within this range are normally conducted. Fig. 9(a) displays the frequency spectrum produced by SVPWM. This modulation technique does not produce significant harmonics at low frequencies, but it does do so at the switching frequency and its multiples. Fig. 9(b) depicts the frequency spectrum of VSFPWM. The first 40 harmonics are similar than those of SVPWM. From 1 to 100 kHz, this modulation produces the lowest distortion among the studied techniques. From 100 kHz onward, the harmonics increase since the converter switches between 100 and 200 kHz. From 150 kHz, there are significant harmonics at the multiples of the switching frequencies. Fig. 9(c) plots the frequency spectrum of H-ΣΔ. The first 40 harmonics are lower than those of SVPWM, but after 40 kHz, some harmonics are somewhat higher than −40 dB. At high frequencies (>150 kHz), nearly all the harmonics are properly mitigated. This behavior originates from the variable switching frequency that spreads the harmonics over noncritical frequencies. Hence, H-ΣΔ is better than SVPWM for complying with the above-mentioned standards. Finally, Fig. 9(d) depicts the line-voltage frequency spectrum produced by DH-ΣΔ. This spectrum is similar to that of H-ΣΔ. However, this technique produces some differences in the frequency domain: at up to 2 kHz, the harmonics are the lowest among the studied techniques; at 35 kHz, harmonics greater than −40 dB begin to appear; then from 150 kHz onward, this modulation presents slightly lower harmonics than H-ΣΔ.

Fig. 10 compares the voltage THD produced by the SVPWM, VSFPWM, and ΣΔ techniques at different frequencies. The voltage THD measurement considers only the first 40 harmonics, as detailed in the standard EN 50160 [43]. Fig. 10(a) plots the results at 100 kHz. At 100 kHz, the SVPWM always exhibits better THD than those of H-ΣΔ. The VSFPWM technique shows THD similar to those of SVPWM. Thus, this technique also produces less distortion than H-ΣΔ. The H-ΣΔ modulation shows the worst THD among all the studied techniques. However, DH-ΣΔ shows better THD than SVPWM for all the operating points. From $m = 0.9$ upward, the distortions of DH-ΣΔ are similar to those of SVPWM. Fig. 10(b) depicts the THD produced at 200 kHz. As the maximum frequency increases, the distortion of PWM techniques grows due to their higher carrier sideband harmonics [46], whereas the THD decreases using both ΣΔ modulations. Increasing the oversampling frequency in ΣΔ modulations enhances the effective number of bits; thus, the resolution grows [23], and the distortion decreases. Hence, the ΣΔ techniques show better THD at this frequency for all operating points. Among ΣΔ techniques, DH-ΣΔ always produces less distortion than H-ΣΔ.

IV. Experimental Results

To experimentally evaluate the proposed modulation techniques for the VSC converter in Fig. 1, we used a scaled-down prototype that incorporated the previously simulated SiC MOSFETs (CCS050M12CM2). On the ac side, there was a three-phase series-connected *RL* load with $R = 68\ \Omega$ and $L = 1.55$ mH. The dc side of the converter was supplied by a constant 300-Vdc source. The modulation techniques were implemented on a dSPACE DS1006 platform and a DS5203 FPGA board. Voltages and currents were measured with a high-resolution

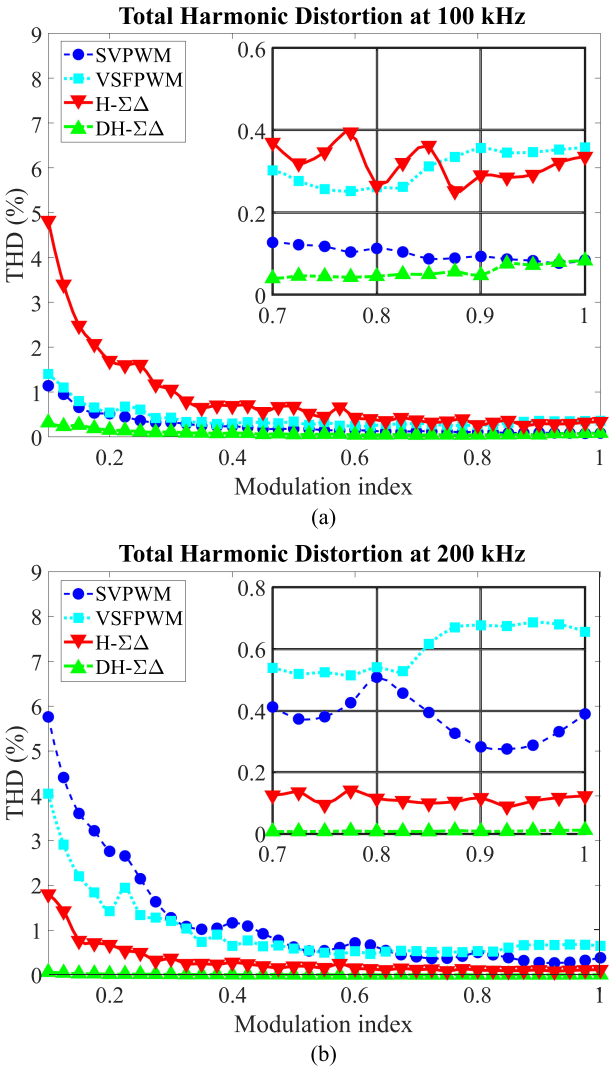

Fig. 10. Comparison of line-voltage THD (V_{ab}) at (a) $f_{\max} = 100$ kHz and (b) $f_{\max} = 200$ kHz.

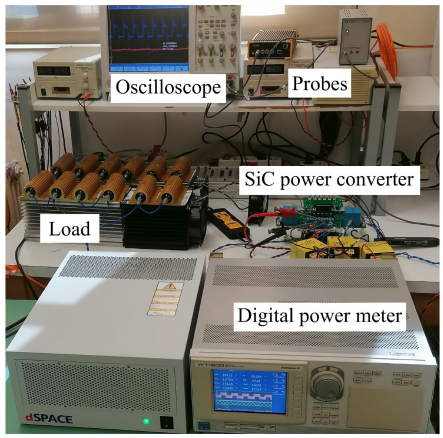

Fig. 11. View of the VSC and the experimental setup.

oscilloscope (Agilent InfiniiVision MSO7104A: 1-GHz bandwidth and 4-GS/s sample rate), high voltage differential probes (PMK BumbleBee: 400-MHz bandwidth), and current probes (Keysight N2783B: 100-MHz bandwidth). The obtained data are processed with MATLAB software to calculate the THD and the voltage frequency spectrum. The converter efficiency was measured using a digital power meter (Yokogawa WT1600: 1-MHz bandwidth). Fig. 11 shows the experimental setup.

A. Experimental Performance

To evaluate the power loss reduction in H-ΣΔ and DH-ΣΔ, we measured the efficiency of the different techniques. Fig. 12 shows the converter efficiency when using the four techniques at 20, 100, and 200 kHz. Fig. 12(a) illustrates the converter performance at 20 kHz. At this frequency, the performance of SVPWM and VSFPWM increases along with the modulation index, but the operating point barely affects the ΣΔ techniques. The efficiency of both ΣΔ techniques is similar and always greater than 93%. Fig. 12(b) depicts the efficiency at 100 kHz. Under this operating condition, the efficiency of both PWM techniques considerably decreases, especially at low modulation indexes. The same statement is true for H-ΣΔ and DH-ΣΔ, but drop in efficiency is less significant. At this frequency, the performance of the four techniques increases with the modulation index. Both ΣΔ techniques show similar performances for modulation indexes greater than 0.4, but H-ΣΔ shows slightly better efficiency for all the operating points. The efficiency difference among the studied techniques reaches a minimum for high modulation indexes. At these indexes, SVPWM shows a performance of around 90% and VSFPWM exhibits an efficiency of 91%. Both ΣΔ modulations have efficiencies greater than 95%. Finally, Fig. 12(c) plots the results at 200 kHz. At this frequency, the four techniques have the same behavior as at 100 kHz. All the modulations are less efficient at 200 kHz because of their higher number of switchings. However, the difference between the efficiency of the SVPWM, VSFPWM, and ΣΔ techniques is more significant. In this scenario, the maximum efficiency of SVPWM is around 80%, whereas both ΣΔ modulations have a maximum performance somewhat higher than 91%. VSFPWM always shows better efficiency than SVPWM, but its maximum efficiency is 82.2%. H-ΣΔ has a higher efficiency than DH-ΣΔ for all the operating points. However, this efficiency difference decreases as the modulation index increases. At high modulation indexes, the difference between ΣΔ modulations is around 1%.

B. Experimental Harmonic Distortion

In order to analyze the quality of ΣΔ modulations, we compared the line voltages and output currents produced by these two techniques with those obtained from the PWM techniques. The frequency spectrum of the line voltages (V_{ab}) obtained at $f_{\max} = 200$ kHz and $m = 0.8$ are depicted in Fig. 13(a). All the experimental spectra are comparable to those obtained by simulation (see Fig. 9). The four techniques show low distortion, of less than -40 dB at frequencies up to 2 kHz. Both ΣΔ techniques exhibit slightly lower distortion than PWM modulations, but DH-ΣΔ shows the best quality at those low frequencies. Between 2 and 150 kHz, the spectra of PWM modulations have

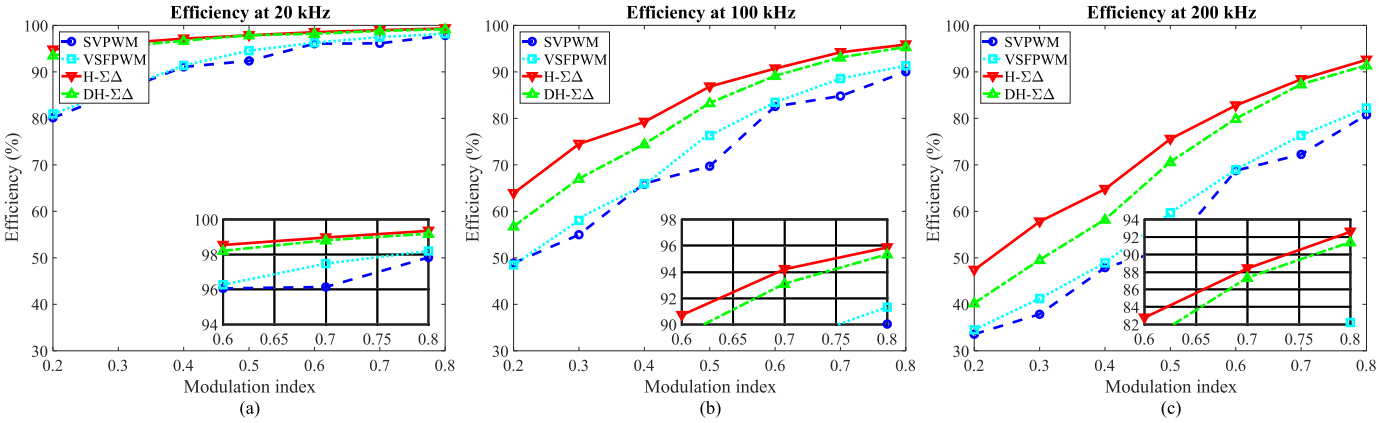

Fig. 12. Converter efficiency curves at (a) $f_{\max} = 20$ kHz, (b) $f_{\max} = 100$ kHz, and (c) $f_{\max} = 200$ kHz.

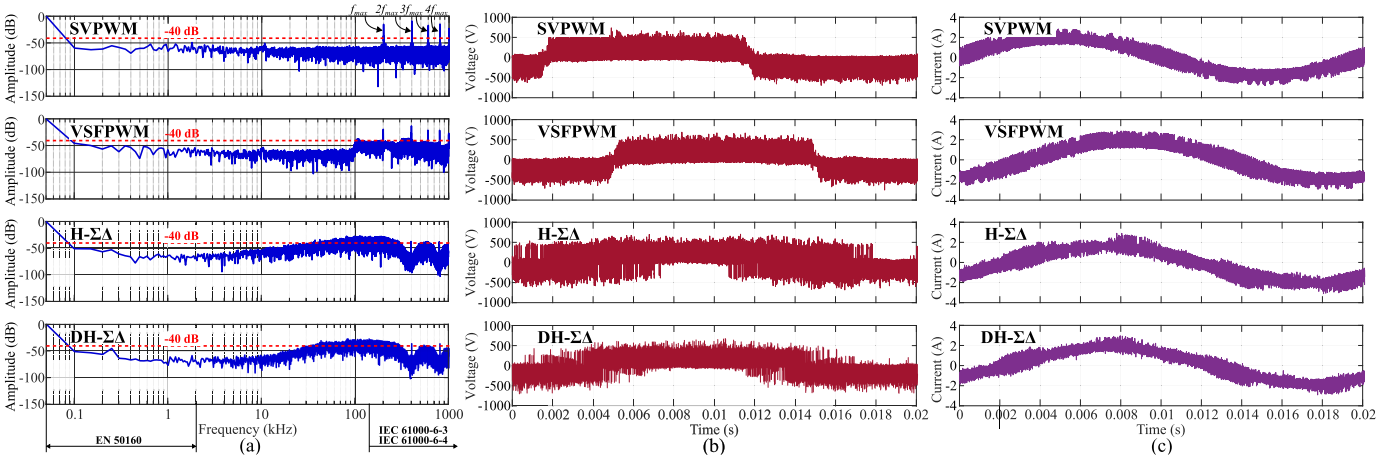

Fig. 13. Experimental results obtained at high frequency (200 kHz) and $m = 0.8$. (a) Frequency spectrum of line voltage (V_{ab}). (b) Line voltage (V_{ab}). (c) Converter output current (I_a).

notable differences compared with those of the ΣΔ techniques. All the harmonics produced by PWM techniques remain below −40 dB, but the distortions of both ΣΔ techniques begin to grow and reach their maximum. The H-ΣΔ spectrum shows that the distortion rises after 4 kHz, whereas the increase in the DH-ΣΔ spectrum begins at 10 kHz. The maximum harmonics of both ΣΔ techniques have comparable values and are somewhat higher than −40 dB. From the maximum switching frequency of 200 kHz onward, SVPWM exhibits significant harmonics at the switching frequency and its multiples, whereas the ΣΔ techniques show much lower harmonics. Since the implemented VSFPWM technique switches from 100 to 200 kHz, it produces more distortion from 100 kHz onward. However, this technique generates smaller harmonics than the SVPWM at the maximum switching frequency and its multiples. There are no notable differences between H-ΣΔ and DH-ΣΔ within this frequency range.

Fig. 13(b) depicts the line voltages (V_{ab}) produced by the four studied techniques. PWM voltages have a cleaner waveform than the others. Some distortion appears in all of them, but it is more notable for the H-ΣΔ and DH-ΣΔ techniques, both of which spread the harmonics over a wide frequency range. Moreover, ΣΔ modulations may switch two phases at once and, thus, produce some voltage spikes.

Fig. 13(c) illustrates the converter output current. All the techniques produce a sinusoidal current and, hence, all of them work correctly. The distortion is also similar for all the currents, so there are no notable differences between them.

In order to confirm the better harmonic distortion of ΣΔ modulations at low frequencies, the THD of the different techniques has been calculated from the obtained measurements. Fig. 14 illustrates the line-voltage THD when using the studied techniques for different maximum frequencies. As described by the standard EN 50160, all the harmonics of up to 2 kHz have been computed [43]. At 20 kHz, the THD of SVPWM is below 1% for all the operating points, whereas the THD of both ΣΔ techniques is extremely high. The severe distortion of ΣΔ techniques has limited their applicability in power converters until the present, now that WBG devices allow switching at higher frequencies. However, the distortion of DH-ΣΔ considerably decreases with the modulation index. At high indexes, its THDs are similar to those of VSFPWM. At 100 kHz, the THD of PWM

TABLE I
DETAIL OF THE EXPERIMENTAL RESULTS

Maximum frequency (f_{max})	Modulation technique	Efficiency (%) Modulation index 0.2	0.3	0.4	0.5	0.6	0.7	0.8	THD (%) Modulation index 0.2	0.4	0.6	0.8
20 kHz	SVPWM	80.12	85.70	91.07	92.36	96.06	96.14	97.83	0.26	0.14	0.21	0.11
	VSFPWM	80.98	86.06	91.38	94.57	96.27	97.48	98.20	0.70	0.58	1.86	2.41
	H-ΣΔ	94.78	96.12	97.14	97.86	98.54	98.97	99.35	10.14	4.60	4.44	3.44
	DH-ΣΔ	93.55	95.40	96.71	97.88	98.21	98.81	99.19	5.33	2.52	1.97	1.43
100 kHz	SVPWM	48.88	54.65	65.99	69.71	82.56	84.80	90.03	0.99	0.42	0.33	0.28
	VSFPWM	48.46	58.09	65.16	76.31	83.45	88.56	91.32	2.07	0.94	0.85	0.84
	H-ΣΔ	63.89	74.49	79.23	86.84	90.71	94.21	95.87	2.01	0.94	0.72	0.49
	DH-ΣΔ	56.78	67.03	74.46	83.31	89.16	91.11	95.35	1.08	0.33	0.33	0.28
200 kHz	SVPWM	33.57	37.87	47.90	52.09	68.76	72.25	80.77	3.63	1.90	1.14	0.82
	VSFPWM	34.53	41.25	48.91	56.69	68.98	76.33	82.22	3.67	1.55	1.09	1.31
	H-ΣΔ	47.40	57.79	64.78	75.56	82.77	88.40	92.59	1.86	0.79	0.66	0.41
	DH-ΣΔ	40.26	49.57	58.25	70.64	79.93	87.34	91.41	0.98	0.23	0.23	0.18

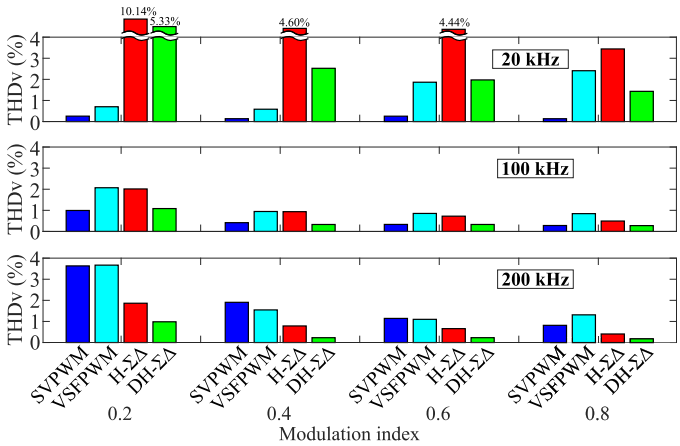

Fig. 14. THD of line voltage (V_{ab}) at 20, 100, and 200 kHz.

modulations are slightly higher, but they decrease as the modulation index increases. Moreover, the THD of both ΣΔ techniques is much better than at 20 kHz. H-ΣΔ exhibits similar distortion than VSFPWM for all the operating points, but DH-ΣΔ shows THDs that are comparable to those of SVPWM. Nonetheless, SVPWM continues to generate the lowest harmonic distortion. At 200 kHz, the THD of both PWM techniques is somewhat higher than at 100 kHz for all the operating points. H-ΣΔ has lower THDs than at 100 kHz for all the studied modulation indexes, and DH-ΣΔ presents about the same distortion levels. At this frequency, DH-ΣΔ is the best option in terms of distortion, closely followed by H-ΣΔ. Both ΣΔ techniques produce less THD than SVPWM and VSFPWM do. Thus, at 200 kHz, the situation is the opposite of what occurs at 20 kHz.

Table I presents in detail the experimental results shown by Figs. 12 and 14.

V. CONCLUSION

This article proposes using H-ΣΔ and DH-ΣΔ for VSCs that use WBG power devices. The proposed ΣΔ modulations are an alternative to SVPWM and other variable switching frequency techniques, for high-frequency operations. The effectiveness of the proposed techniques is demonstrated by the experimental results. Both ΣΔ modulations are compared to the conventional SVPWM technique and a variable switching frequency SVPWM at different frequencies. The results show that ΣΔ techniques do not have significant advantages for low-frequency operations, such as those of IGBTs. Nevertheless, H-ΣΔ and DH-ΣΔ exhibit salient features for high-frequency operations when compared with the PWM techniques. The experiments demonstrate that both ΣΔ modulations decrease power losses and, thus, improve converter efficiency. Moreover, the proposed techniques reduce the low-order harmonics, such that the THDs of these techniques are lower than those produced by SVPWM. ΣΔ modulations also generate smaller high-order harmonics than PWM techniques. Finally, this article concludes that the effectiveness and the benefits of H-ΣΔ and DH-ΣΔ increase in parallel with the operating frequency.

REFERENCES

[1] J. Millan, P. Godignon, X. Perpina, A. Perez-Tomas, and J. Rebollo, "A survey of wide bandgap power semiconductor devices," *IEEE Trans. Power Electron.*, vol. 29, no. 5, pp. 2155–2163, May 2014.
[2] K. Shenai, "High-density power conversion and wide-bandgap semiconductor power electronics switching devices," *Proc. IEEE*, vol. 107, no. 12, pp. 1–19, Nov. 2019.
[3] H. Dong *et al.*, "Progress of power field effect transistor based on ultra-wide bandgap Ga2O3 semiconductor material," *IEEE Trans. Power Electron.*, vol. 35, no. 5, pp. 5157–5179, May 2020.
[4] I. López, E. Ibarra, A. Matallana, J. Andreu, and I. Kortabarria, "Next generation electric drives for HEV/EV propulsion systems: Technology, trends and challenges," *Renewable Sustain. Energy Rev.*, vol. 114, 2019, Art. no. 109336.
[5] K. Dang *et al.*, "A 5.8 GHz high-power and high-efficiency rectifier circuit with lateral GaN Schottky diode for wireless power transfer," *IEEE Trans. Power Electron.*, vol. 35, no. 3, pp. 2247–2252, Mar. 2020.
[6] T. Mishima and E. Morita, "High-frequency bridgeless rectifier based ZVS multiresonant converter for inductive power transfer featuring high-voltage GaN-HFET," *IEEE Trans. Ind. Electron.*, vol. 64, no. 11, pp. 9155–9164, Nov. 2017.
[7] B. Li, Q. Li, F. C. Lee, Z. Liu, and Y. Yang, "A high-efficiency high-density wide-bandgap device-based bidirectional on-board charger," *IEEE J. Emerg. Sel. Topics Power Electron.*, vol. 6, no. 3, pp. 1627–1636, Sep. 2018.
[8] H. Li *et al.*, "A 30-kHz 6.6-kW SiC bidirectional LLC onboard charger," *IEEE Trans. Ind. Electron.*, vol. 67, no. 2, pp. 1435–1445, Feb. 2020.

[9] F. Xue, R. Yu, and A. Q. Huang, "A 98.3% efficient GaN isolated bidirectional storage system applications," *IEEE Trans. Ind. Electron. Ind. Electron.*, vol. 64, no. 11, pp. 9094–9103, Nov. 2017.
[10] A. N. Lemmon, R. Cuzner, J. Gafford, R. Hosseini, A. D. Brovont, and M. S. Mazzola, "Methodology for characterization of common-mode conducted electromagnetic emissions in wide-bandgap converters for ungrounded shipboard applications," *IEEE J. Emerg. Sel. Topics Power Electron.*, vol. 6, no. 1, pp. 300–314, Mar. 2018.
[11] A. K. Morya *et al.*, "Wide bandgap devices in AC electric drives: Opportunities and challenges," *IEEE Trans. Transp. Electrific.*, vol. 5, no. 1, pp. 3–20, Mar. 2019.
[12] A. Matallana *et al.*, "Power module electronics in HEV/EV applications: New trends in wide-bandgap semiconductor technologies and design aspects," *Renewable Sustain. Energy Rev.*, vol. 113, Oct. 2019, Art. no. 109264.
[13] S. Ohn *et al.*, "Three-terminal common-mode EMI model for EMI generation, propagation, and mitigation in a full-SiC three-phase UPS module," *IEEE Trans. Power Electron.*, vol. 34, no. 9, pp. 8599–8612, Sep. 2019.
[14] S. Yin, K. J. Tseng, R. Simanjorang, Y. Liu, and J. Pou, "A 50-kW high-frequency and high-efficiency SiC voltage source inverter for more electric aircraft," *IEEE Trans. Ind. Electron.*, vol. 64, no. 11, pp. 9124–9134, Nov. 2017.
[15] R. Gamoudi, D. E. Chariag, and L. Sbita, "A review of spread-spectrum-based PWM techniques—A novel fast digital implementation," *IEEE Trans. Power Electron.*, vol. 33, no. 12, pp. 10292–10307, Dec. 2018.
[16] D. Jiang and F. F. Wang, "Variable switching frequency PWM for three-phase converters based on current ripple prediction," *IEEE Trans. Power Electron.*, vol. 28, no. 11, pp. 4951–4961, Nov. 2013.
[17] J. Chen, D. Jiang, W. Sun, Z. Shen, and Y. Zhang, "An improved variable switching frequency modulation strategy for three-level converters with reduced conducted EMI," in *Proc. IEEE Energy Convers. Congr. Expo.*, 2019, pp. 6937–6942.
[18] L. Wei and R. A. Lukaszewski, "Pulse width modulation (PWM) rectifier with variable switching frequency," Patent US 7,190,143 B2, Mar. 2007.
[19] F. Yang, A. R. Taylor, H. Bai, B. Cheng, and A. A. Khan, "Using d-q transformation to vary the switching frequency for interior permanent magnet synchronous motor drive systems," *IEEE Trans. Transp. Electrific.*, vol. 1, no. 3, pp. 277–286, Oct. 2015.
[20] X. Zhao, X. Wang, S. Liu, C. Gu, S. Zhao, and Z. Deng, "Switching frequency variation based on current ripple analysis of a 3-L PMSM drive system considering neutral point balance," *IET Power Electron.*, vol. 13, no. 4, pp. 776–787, Mar. 2020.
[21] S. Pavan, R. Schreier, and G. C. Temes, *Understanding Delta-Sigma Data Converters*, 2nd ed. Hoboken, NJ, USA: Wiley-IEEE Press, 2017.
[22] E. Janssen and A. van Roermund, *Look-Ahead Based Sigma-Delta Modulation*, 1st ed. Dordrecht, The Netherlands: Springer, 2011.
[23] J. Reiss, "Understanding sigma-delta modulation: The solved and unsolved issues," *J. Audio Eng. Soc.*, vol. 56, no. 1/2, pp. 49–64, Jan. 2008.
[24] J. C. Candy, "A use of double integration in sigma delta modulation," *IEEE Trans. Commun.*, vol. COM-33, no. 3, pp. 249–258, Mar. 1985.
[25] M. Yavari and O. Shoaei, "Low-voltage sigma-delta modulator topologies for broadband applications," in *Proc. IEEE Int. Symp. Circuits Syst.*, 2004, pp. 964–975.
[26] G. Luckjiff, I. Dobson, and D. Divan, "Interpolative sigma delta modulators for high frequency power electronic applications," in *Proc. Power Electron. Spec. Conf.*, 1995, pp. 444–449.
[27] I. H. Kheraluwala and D. M. Divan, "Delta modulation strategies for resonant link inverters," *IEEE Trans. Power Electron.*, vol. 5, no. 2, pp. 220–228, Apr. 1990.
[28] A. Mertens, "Performance analysis of three-phase delta-modulation systems," *IEEE Trans. Ind. Appl.*, vol. 30, no. 4, pp. 1016–1027, Aug. 1994.
[29] A. Hirota, S. Nagai, and M. Nakaoka, "A novel delta-sigma modulated space vector modulation scheme using scalar delta-sigma modulators," in *Proc. IEEE 34th Annu. Conf. Power Electron. Spec.*, 2003, pp. 485–489.
[30] A. Hirota, B. Saha, S. P. Mun, and M. Nakaoka, "An advanced simple configuration delta-sigma modulation three-phase inverter implementing space voltage vector approach," in *Proc. IEEE Power Electron. Spec. Conf.*, 2007, pp. 453–457.
[31] Deepakraj M. Divan, I. Dobson, and G. A. Luckiff, "Modulator for resonant link converters," Patent 5,619,406, Apr. 8, 1997.
[32] G. Luckjiff and I. Dobson, "Power spectrum of a sigma-delta modulator with hexagonal vector quantization and constant input," in *Proc. IEEE Int. Symp. Circuits Syst.*, 1999, pp. 270–273.
[33] G. Luckjiff and I. Dobson, "Hexagonal sigma–delta modulation," *IEEE Trans. Circtuits Syst.*, vol. 50, no. 8, pp. 991–1005, Aug. 2003.
[34] G. Luckjiff and I. Dobson, "Hexagonal ΛΔ modulators in power electronics," *IEEE Trans. Power Electron.*, vol. 20, no. 5, pp. 1075–1083, Sep. 2005.
[35] J. Nieznanski, A. Wojewodka, and P. J. Chrzan, "Comparison of vector sigma-delta modulation and space-vector PWM," in *Proc. 26th Annu. Conf. IEEE Ind. Electron. Soc.*, 2000, pp. 1322–1327.
[36] B. Jacob and M. R. Baiju, "Spread spectrum scheme for two-level inverters using space vector sigma-delta modulation," in *Proc. 5th IET Int. Conf. Power Electron., Mach. Drives*, 2010, pp. 1–6.
[37] B. Jacob and M. R. Baiju, "Spread spectrum scheme for three-level inverters based on space vector sigma delta modulator," in *Proc. IEEE Int. Symp. Ind. Electron.*, 2010, pp. 1491–1496.
[38] B. Jacob and M. R. Baiju, "Vector-quantized space-vector-based spread spectrum modulation scheme for multilevel inverters using the principle of oversampling ADC," *IEEE Trans. Ind. Electron.*, vol. 60, no. 8, pp. 2969–2977, Aug. 2013.
[39] B. Jacob and M. R. Baiju, "A new space vector modulation scheme for multilevel inverters which directly vector quantize the reference space vector," *IEEE Trans. Ind. Electron.*, vol. 62, no. 1, pp. 88–95, Jan. 2015.
[40] J. Kabziński, *Advanced Control of Electrical Drives and Power Electronics*, vol. 75. Cham, Switzerland: Springer, 2017.
[41] A. Land and A. Doig, "An automatic method of solving discrete programming problems," *Econometrica*, vol. 28, no. 3, pp. 497–520, Jun. 1960.
[42] *PLECS User Manual*, 4th ed., Plexim GmbH, Zurich, Switzerland, 2019.
[43] *Voltage Characteristics of Electricity Supplied by Public Electricity Networks*, EN 50160:2010, 2010.
[44] *Electromagnetic Compatibility (EMC). Part 6-3: Generic Standards. Emission Standard for Residential, Commercial and Light-Industrial Environments. (IEC 61000-6-3:2006)*, EN 61000-6-3:2007, 2007.
[45] *Electromagnetic Compatibility (EMC). Part 6-4: Generic Standards. Emission Standard for Industrial Environments. (IEC 61000-6-4:2006)*, EN 61000-6-4:2007, 2007.
[46] D. G. Holmes, "General analytical method for determining the theoretical harmonic components of carrier based PWM strategies," in *Proc. IAS Annu. Meeting Conf. Rec. IEEE Ind. Appl. Conf.*, 1998, vol. 2, no. 2, pp. 1207–1214.

David Lumbreras (Graduate Student Member, IEEE) received the B.S. degree in industrial technology engineering and the M.S. degree in automatic systems and industrial electronics engineering, in 2017 and 2018, respectively, from the Technical University of Catalonia (UPC), Barcelona, Spain, where he is currently working toward the Ph.D. degree in electronic engineering with the Terrassa Industrial Electronics Group, Department of Electronic Engineering, UPC, Terrassa, Spain.

From July 2016 to January 2019, he was a CE Marking Engineer with the Certification Unit of Applus+ Laboratories Bellaterra, Spain. Since 2019, he has been a Researcher with the R&D Power Electronics, Circutor S.A., Viladecavalls, Spain. His research interests include modeling and control of power converters, multilevel converters, power quality, renewable energy, active power filters, electromagnetic compatibility, and modulation techniques.

Jordi Zaragoza (Member, IEEE) received the B.S. degree in electronic engineering, the M.S. degree in automatic and electronic industrial engineering, and the Ph.D. degree from the Technical University of Catalonia (UPC), Catalonia, Spain, in 2001, 2004, and 2011 respectively.

In 2003, he joined as an Assistant Professor with the Faculty of UPC, where he became an Associate Professor in 2012. From 2006 to 2007, he was a Researcher with the Energy Unit of ROBOTIKER-TECNALIA Technologic Corporation, Basque Country, Spain. Since 2017, he has been the Director of the Terrassa Industrial Electronics Group, UPC. He is the author of more than 70 published technical papers and has been involved in several projects in the fields of power electronics and systems. His research interests include modeling and control of power converters, multilevel converters, wind energy, power quality, and HVdc transmission systems.

Néstor Berbel (Member, IEEE) received the B.S., M.S., and Ph.D. degrees from the Technical University of Catalonia (UPC), Barcelona, Spain, in 2002, 2004, and 2015, respectively, all in electronic engineering.

In 2003, he joined as an Assistant Professor with the Faculty of UPC, where he became an Associate Professor in 2012. His scientific research has been developed at the Terrassa Industrial Electronics Group, Department of Electronic Engineering, UPC, Terrassa, Spain. His research interests include microelectronic reliability, power converters, efficiency on power converters, modulations, and control loops applied on power converters.

Juan Mon was born in Galicia, Spain, in 1977. He received the M.S. and Ph.D. degrees in electronics engineering from the Technical University of Catalonia (UPC), Barcelona, Spain, in 2005 and 2012, respectively.

In 2000, he joined the Faculty of UPC, as an Assistant Professor with the Department of Electronics Engineering. His main research interests focus on the electromagnetic compatibility in power converters.

Eduardo Gálvez was born in Sevilla, Spain. He received the M.S. degree in telecomunications engineering from the Technical University of Valencia (UPV), Valencia, Spain, in 2000.

From 2000 to 2002, he was a Probe Test Engineer with Analog Devices, Limerick, Ireland. From 2003 to 2005, he was an Electronic Products Supplier Quality Engineer with Ficosa, Barcelona, Spain. Since 2005, he has been with Circutor S.A., Viladecavalls, Spain, as a Development Engineer with Zurc Development Center. From 2010 to 2015, he was an Engineering Manager of Zurc, where he has been a Power Electronics Engineering Manager with the Circutor Development Center since 2014. He also holds two patents.

Alfonso Collado received the B.S. degree in electronics engineering from the Technical University of Catalonia (UPC), Barcelona, Spain, in 1989.

From 1986 to 1989, he was a Research Technician with Instrumentacion Industrial Zurc, Viladecavalls, Spain, where he become a Technical Manager from 1989 to 2010. Since 2010, he is an R&D&i Manager with Circutor S.A., Viladecavalls, Spain. For the last three years, he has been working specially in innovative technologies and how to apply these to the new products developed by the company. His main research interests include energy efficiency, power conversion efficiency, renewable energy, electric vehicles, and the new IoT opportunities to improve the consumer's behavior about how to be more efficiency managing his consumptions.